The use of tungsten yarns in the production for W_f/W

J.W.Coenen[a,*], M.Treitz[a], H.Gietl[b,c],P.Huber[d], T.Hoeschen[b], L.Raumann[a], D.Schwalenberg[a], Y.Mao[a], J.Riesch[b], A.Terra[a], Ch.Broeckmann[e] O.Guillon[a], Ch.Linsmeier[a], R.Neu[b,c]

[a]Forschungszentrum Jülich GmbH, Institut für Energie- und Klimaforschung 52425 Jülich, Germany
[b]Max-Planck-Institut für Plasmaphysik, 85748 Garching, Germany
[c]Technische Universität München, 85748 Garching, Germany
[d]Institut für Textiltechnik (ITA) der RWTH Aachen University, Aachen, Germany
[e]Lehrstuhl für Werkstoffanwendungen im Maschinenbau, RWTH Aachen, 52062 Aachen, Germany

E-mail: j.w.coenen@fz-juelich.de

Abstract. Material issues pose a significant challenge for the design of future fusion reactors. Recently progress has been made towards fully dense multi short-fibre powder metallurgical production of tungten-fibre reinforced tungsten (W_f/W) as well as optimising the process understanding for the routes using chemical vapor deposition (CVD). For CVD-W_f/W weaves and textile preforms are being used to facilitate large scale production. Classically 150 μm tungsten fibres supplied by OSRAM GmbH have been used. In order to facilitate the better use of textile processes less stiff 16 μm filaments are being evaluated. The strength of the 16 μm flament is at 4500 MPa and thus significantly higher than the strength of the 150 μm fibre (∼2500 MPa) (in the as-fabricated state). Better weavability allows a more flexible use of fibre preforms. Two main yarn production routes have been investigated: covered yarns where a set of tungsten filaments is held together by a PVA (Polyvinyl alcohol) cover and braided yarns. In oder to allow a comparison to the previously used single fibres, yarns with $\sim 140\,\mu m$ effective diameter were produced. Braided yarns with tensile strength of 2500 MPa and 6% strain at fracture and twisted yarns with tensile strength of 4500 MPa and 3% strain at fracture. For both yarns single fibre CVD samples have been produced to investigate the infiltration properties of the yarns and thus their applicability for the CVD route. A dense infiltration is observed for all yarns under investigation.

1. Introduction

Solid Tungsten (W) is currently the only viable candidate for uses as plasma facing material in the highly loaded divertor components of any future fusion reactor. As tungsten is resilient against erosion by impinging plasma ions and neutrals, has the

highest melting point of any metal, and shows rather benign activation behavior under neutron irradiation. In addition, low tritium retention is a beneficial property. In recent years many of studies have tackled the issue to qualify current materials with respect to these issues for ITER ‡[1, 2, 3, 4, 5, 6, 7, 8, 9, 10, 11, 12] and beyond. For a DEMO § type device, or a future fusion power plant the limits are more stringent. It is assumed that the boundary conditions [2, 13] to be fulfilled for the materials are in many cases above the technical feasibility limits as they are set out today [10, 11].

New advanced-options for use as PFCs are being developed (see [14, 15, 16, 17, 8], and references therein) focussing on crack resilient composites with low activation, now or low tritium uptake, enhanced lifetime and low erosion. Many advanced materials base their improved properties on the use of a composite approach. Figure 1 visualises the effect of such an approach. In 1 (a), the stress-strain behaviour of a fully brittle material is given. Failure occurs in a sudden manner, immediately at ultimate tensile strength (UTS). In (b), a material showing a slow crack growth is given, characteristic is the transition from branch I to branch II, with a decreasing slope. Material (c), is failure tolerant, with no sudden failure and remaining load bearing capability, beyond UTS.

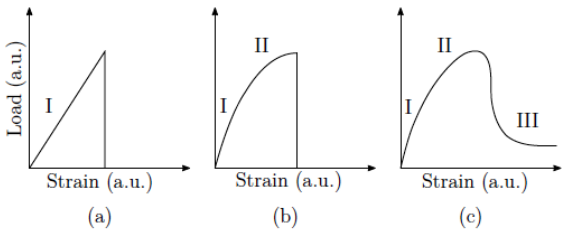

Figure 1: Prospect of Metal Matrix Copmposite (MMC) development,based on [18]

.

Characteristic for this material behaviour is the existence of three distinct branches

‡ https://www.iter.org
§ https://www.euro-fusion.org/programme/demo/

in the stress-strain curve: branch I with proportionality between stress and strain, branch II being the domain of matrix cracking and finally branch III showing extensive load drop, but remaining load bearing capacity. This behaviour is found in long fibre reinforced composites, being equipped with well-engineered and weak interfaces, providing de-bonding and fibre pull-out in the event of fracture [18, 19]. As a result energy dissipating mechanisms like ductile deformation of fibres, crack bridging and deflection are facilitated [20, 21, 22]. The key-functions of strengthening and toughening

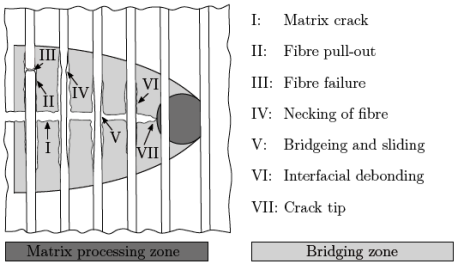

Figure 2: Mechanisms of crack propagation & energy dissipation [23, 24].

are assigned to the fibre matrix interface: strengthening results from the load transfer between fibre and matrix, whereas toughening depends on energy dissipation and absorption mechanisms [25].

The local fracture of the interphase component plays a major role in the material properties, a crack moving through the matrix will propagate through the cross-section unhampered, if no de-bonding and crack deflection occurs. If crack deflection is successfully induced, debonding, crack bridging and fibre pull-out occur and consequently increase the fracture toughness by external energy dissipation [26]. Figure 2 shows the typical mechanisms.

In this contribution the focus lies on the introduction of a new class of tungsten yarns and to be used in textile preforms for W_f/W as described in [27]. The properties of the individual yarns, their structure and infiltration behaviour are being discussed. The yarns are meant to provide beneficial influence on the overall material properties

and pseudo-ductile behaviour. Particular as the strength of the wires increases with decreasing diameter as already shown in [27].

2. Tungsten-Fibre Reinforced Tungsten

To overcome the brittleness issues when using W, a W fibre reinforced W composite material (W_f/W), incorporating extrinsic toughening mechanisms as described above can be used.

Various methods of building and constructing W_f/W composites, either via Chemical Vapor Deposition (CVD) [28, 29, 30] or powder metallurgical (PM) processes [31, 32] are available. Based on the work presented here and previously in [14, 27, 31, 33, 34, 35, 36, 37], the basic proof of principle for CVD & PM-W_f/W has been achieved. Fully dense material is aimed for and porosity will diminish mechanical properties as much as behaviour with respect to fuel retention. One of the crucial issues is to maintain as much of the properties of the constituents even after exposing the material to the production cycle and the fusion environment allowing for optimal extrinsic toughening and pseudo-ductile behaviour. Here mainly the adapted interface and the strength of the fibre as well as the preform [27] are important. Yttria is an ideal candidate as the interface material for the W_f/W composite due to its several advantageous properties: good thermal and chemical stability, high mechanical strength and hardness [38, 39] as well as low neutron activation. The preforms are currently produced based on 150 μm fibres, and the process parameters are based on experience. To improve the CVD W_f/W material multiple avenues can be pursued - improving the textile preform and improving the CVD matrix production are among the most promising ones. With respect to the constituent properties potassium doped W-wires can mitigate temperature induced embrittlement effects and thus retain their ductility

even at elevated temperatures (above 1500 K) [34]. The mechanisms, including ductile fibre deformation, necessary for pseudo-ductility will be retained [38, 35, 37]. Properties of the fibres can however be degraded by various circumstances e.g. by impurities during fabrication [40, 41], high-temperatures or neutron irradiation during operation [42, 43]. To maintain the wires properties also improved fibre types e.g. yarns can contribute by introducing better properties e.g. tensile strength at the point of production. The strength of the 16 μm flament is at 4500 MPa and thus significantly higher than the strength of the 150 μm fibre (∼2500 MPa) (in the as-fabricated state). During the CVD process, the improvement of the W_f/W properties can be realised by optimising the process parameters, fiber sizing, and fiber positioning, with respect to fiber volume fraction, relative density, and WF_6 consumption. For this purpose, a model simulation

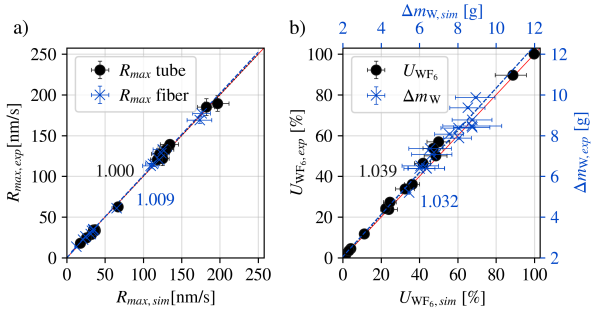

Figure 3: Overview of experimental vs. simulated results; a) max. W deposition rates $R_{W,max}$; b) consumption rates U_{WF_6} and W mass gains Δm_W [30].

.

work has been performed by using COMSOL. The kinetics for the model were validated experimentally (Fig. 3) resulting in a new rate equation, as described in [30]. This allows for a more precise infiltration of even complex structures as yarns.

3. Tungsten Yarns

For the purpose of this work two main types of yarns are being used - covered yarn as well as braided yarn. A covered yarn, subsequently called enwinded yarn, is a yarn,

consisting of a core and sleeve filaments. Both can be substantially different in material and structure. Twisting is applied during fabrication to impart cohesion to the filament bundle. Depending on the twist-level, the surface structure can be altered. Enwinding exerts a transversal force on the fibre bundle and increases strength. Covering of the individuak filaments can be performed as single or double layer. The latter is performed with alternating twist direction, to suppress curling of the yarn. For the twisted enwound yarn the following choices were made: 19 Filaments were fed into the enwinding machine in parallel. The fibres were enwound by a removable multifilament (PVA) and the number of twists per meter were varied (0, 200, 400, 600, 800, 1000). The procedure is shown in 4 (a). The enwinded yarn was fabricated with an enwinding machine, type Allma ESP2, from Saurer AG, Watwill, Switzerland. The filaments were enwound by a removable multifilament type Solvron SF 110T/25F, NITIVY CO. LTD, Tokyo.

The parameter variations are summarized in Tab. 1.

Table 1: Parameter for enwinded yarn fabrication.

Parameter	**Value**	**Unit**
Twist number	0-1000	tw/m
Rotational speed hollow spindle	1600-8000	rpm
Creep Speed	5	m/min
Fast gear	8	m/min
Number of filaments	19	-

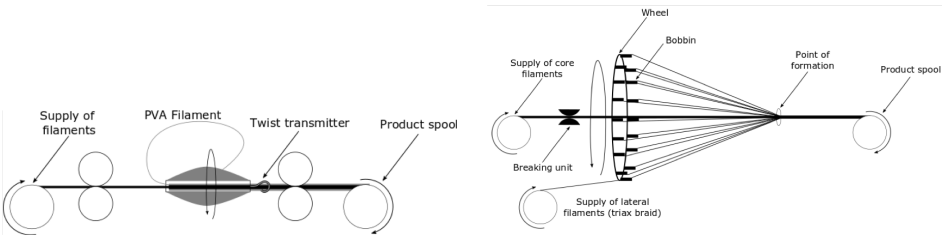

(a) Schematic of a enwinding machine

(b) Schematic of radial braiding machine

Figure 4: Procedures for enwinding (a) and braiding (b).

Braided yarns are based on braiding as a very versatile textile process, that offers various possible variation of the braid and the machine itself. Only the process of radial braiding is relevant for the work presented. Based on the process shown in 4 (b) the following yarn types are considered here: Biaxial Braided Yarn (16 Filaments); Triaxial Braided Yarns with overbraiding of core filaments (16 + 7 Filaments). For both yarn types the typical geometry is given below. The braided yarn structures were fabricated on a type HS 80/48 braiding machine from Körting, Nachfolger Wilhelm Steeger GmbH & Co. KG, Wuppertal. 16 carriers were used and the braid pattern was selected to "one over two under two" The brading angle was adjusted to 45°.

(a) Yarn structure of enwinded yarn

(b) Biaxial braid (only filaments in the sleeve (s))

(c) Triaxial braid (sleeve (s) and non-interlaced core filaments (c))

Figure 5: Structures of the utilized yarns.

Based on the scheme presented in Fig. 5 yarns with various twist numbers and surfaces as well as core filaments have been produced. Examples for their structures are presented in Fig. 6.

For the braided yarns only two types are shown. $R.B.\,16_S$ with 16 surface filaments only and $R.B.\,16_S + 7_c$ with additional 7 core filaments (here R.B. stand for Radial Braid).

Clearly the different structure of both the enwinded yarn as well as the braid is visible. The yarns have been evaluated as produced with respect to their properties. The stress-strain behaviour of the different yarn structures shows a clear dependence of the fabrication process, respectively the resulting yarn structure, in respect to the

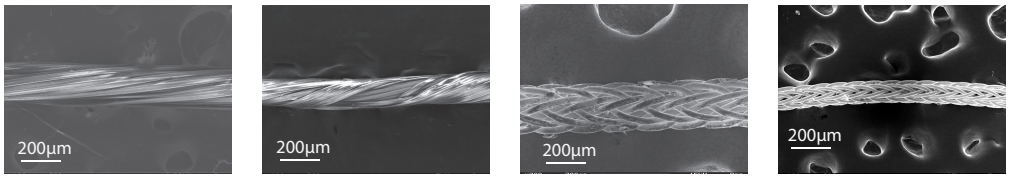

(a) 'ENW. 200 tw/m' (b) 'ENW. 1000 tw/m' (c) 'R.B. 16_s + 7 $_c$' (200x) (d) 'R.B. 16_s'

Figure 6: Enwinded tungsten filament yarns (a), (b) & braided and twisted tungsten filament yarns (c), (d). Here ENW stands for enwinded yarn, R.B. stand for Radial Braid, and 200-1000 is the number of twists per meter put onto the yarn during production.

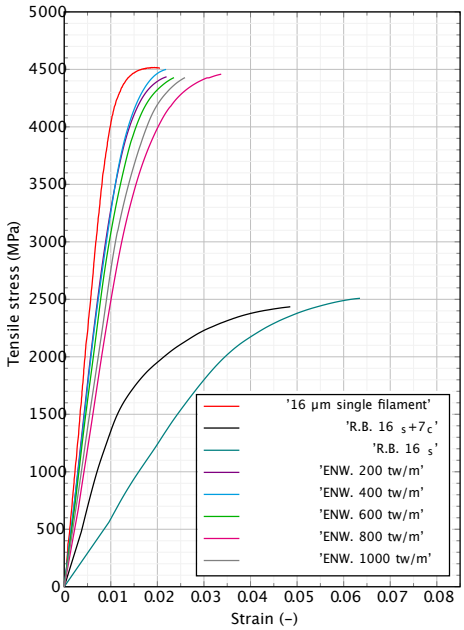

Figure 7: Average stress-strain curves of as produced yarns and a single fibre for comparison. Typically 4 tests were performed and averaged.

arrangement of the filaments and yarn structure. The averaged stress-strain curves are given in Fig. 7.

The yarns of type ('ENW.') show only slightly reduced fracture strength, compared to a thin single filament and only a mild effect of the twisting on the stiffness (increase), respectively the Young's Modulus of the yarn structure. In contrast to this, the braided yarn structures ('R.B.') show significantly decreased fracture stress (2500 MPa) compared to the 16 μm single filament (4550 MPa), however increased fracture strain

of up to 6 %.

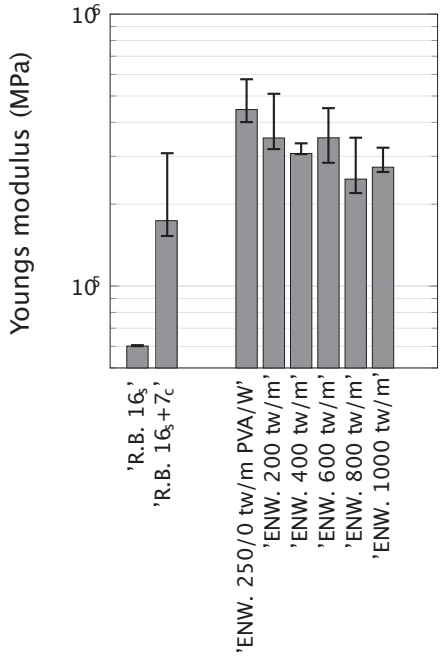

Figure 8: Youngs Modulus for the characterised fibers

Figure 8 shows the difference between the two yarn types, the elastic modulus is particularly low for the braided yarns. Generally, inclination and the amount of inclined filaments affects the yarn structure stiffness to lower values for higher inclination. Based on the results of the tensile properties only the ENW 800 and 1000 as well as the braided yarns are further considered. for the enwinding yarns good cohesion was only achieved at higher twist numbers even-though no major other properties shows significant differences.The surrounding diameter ‖ of all yarn types has the same order of magnitude and is found to varybetween 113.8 and 136.9 μm as shown in Fig. 9 .

4. Infiltration & Testing

For the use in the W_f/W composite the infiltration behaviour of the individual yarns is paramount. Samples for the investigation of the infiltration behaviour were fabricated

‖ imaginary circle encompassing all filaments

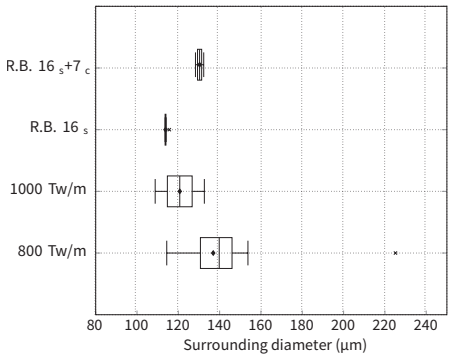

Figure 9: Surrounding yarn diameter after matrix infiltration. Crosses represent outliers.

by longitudinal single fibre infiltration. The yarn was wound around two threaded rods and clamped by pairs of nuts. Subsequently, the yttria interphase coating [39, 33] and the matrix infiltration were performed [34, 30]. The CVD parameters were chosen according to the rate equations given in [30]. 400 sccm WF_6, 2000 sccm H_2 at 100 mbar at 600 $°C$ for 45 minutes.

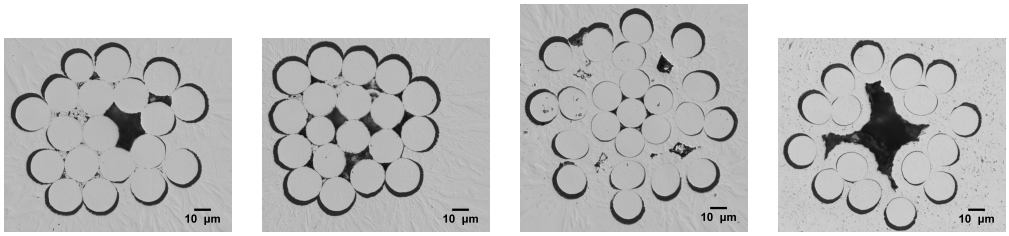

(a) 'ENW. 800 tw/m' (b) 'ENW. 1000 tw/m' (c) 'R.B. 16_s + 7 $_c$' (d) 'R.B. 16_s'

Figure 10: Cross-sectional cuts of infiltrated tungsten filament yarns.

For all yarn types, infiltration into all open cavities is observed (Fig. 10). Generally, convergent structures (considered from the outside of the yarn to the inside) show full infiltration (e.g. bigger openings on the outside of the yanrs and smaller on the inside), whereas at the point of divergence (big openings on the inside and small on the outside), the common CVD-processes related porosity (gap closure) occurs. Generally all surfaces show equal growth rates [30]. Estimating the remaining pore fraction within

the diameter of the yarns leads to numbers between 99 and 99.8%. with the 'R.B. $16_s + 7_c$' showing the least filling.

5. Summary & Outlook

The yarn fabrication by use of industrial textile machines is suitable for the fabrication of filament-based tungsten yarns. Tensile properties of the yarns before and after infiltration have been determined. Enwinded yarns are showing tensile properties similar to the single filaments. Braided yarns are a factor 2 lower but are showing higher strain. The main difference between the enwinded yarn and the braided yarn can be found in the tensile properties. Braided yarns show tensile strength of 2500 MPa and 6% strain at fracture and twisted yarns with tensile strength of 4500 MPa and 3% strain at fracture Investigation of the infiltration behaviour did not reveal any significant differences between the yarn structures, since the gas-phase infiltration reaches the smallest gap between adjacent filaments and infiltrates all open cavities, as long as the gap-closure effect does not block the cavity from the outside.

The next steps include now upscaling of yarn production and production of woven preforms as already available from the standard 150 μm tungsten wires [27].

Acknowledgements

This work has been carried out within the framework of the EUROfusion Consortium and has received funding from the Euratom research and training programme 2014-2018 and 2019-2020 under grant agreement No 633053. The views and opinions expressed herein do not necessarily reflect those of the European Commission

[1] Steven J Zinkle. Applicability of copper alloys for DEMo high heat flux components. *Physica Scripta*, 2016(T167):014004, 2016.

[2] J.H. You, E. Visca, T. Barrett, B. Böswirth, F. Crescenzi, F. Domptail, M. Fursdon, F. Gallay, B-E. Ghidersa, H. Greuner, M. Li, A.v. Müller, J. Reiser, M. Richou, S. Roccella, and Ch. Vorpahl. European divertor target concepts for DEMO: Design rationales and high heat flux performance. *Nuclear Materials and Energy*, 16:1–11, aug 2018.

[3] Y Ueda, JW Coenen, G De Temmerman, RP Doerner, J Linke, V Philipps, and E Tsitrone. Research status and issues of tungsten plasma facing materials for ITEr and beyond. *Fusion engineering and design*, 89(7):901–906, 2014.

[4] R.A. Pitts, S. Carpentier, F. Escourbiac, T. Hirai, V. Komarov, S. Lisgo, A.S. Kukushkin, A. Loarte, M. Merola, A. Sashala Naik, R. Mitteau, M. Sugihara, B. Bazylev, and P.C. Stangeby. A full tungsten divertor for ITEr: physics issues and design status. *Journal of Nuclear Materials*, 438:S48, 2013.

[5] Richard E. Nygren, Ryan R. Dehoff, Dennis L. Youchison, Yutai Katoh, Y. Morris Wang, Charles M. Spadaccini, Charles H. Henager, P. Randall Schunk, David M. Keicher, R. Allen Roach, Mark F. Smith, and Dean A. Buchenauer. Advanced manufacturing—a transformative enabling capability for fusion. *Fusion Engineering and Design*, 136:1007–1011, nov 2018.

[6] A.v. Muller, D. Ewert, A. Galatanu, M. Milwich, R. Neu, J.Y. Pastor, U. Siefken, E. Tejado, and J.H. You. Melt infiltrated tungsten–copper composites as advanced heat sink materials for plasma facing components of future nuclear fusion devices. *Fusion Engineering and Design*, 124:455–459, nov 2017.

[7] C. Linsmeier, B. Unterberg, W. Coenen J., R. Doerner, H. Greuner, A. Kreter, J. Linke, and H. Maier. Material testing facilities and programs for plasma-facing component testing. *Nuclear Fusion*, 57(9):092012, jun 2017.

[8] Ch. Linsmeier, M. Rieth, J. Aktaa, T. Chikada, A. Hoffmann, J. Hoffmann, A. Houben, H. Kurishita, X. Jin, M. Li, A. Litnovsky, S. Matsuo, A. von Müller, V. Nikolic, T. Palacios, R. Pippan, D. Qu, J. Reiser, J. Riesch, T. Shikama, R. Stieglitz, T. Weber, S. Wurster, J.-H. You, and Z. Zhou. Development of advanced high heat flux and plasma-facing materials. *Nuclear Fusion*, 57(9):092007, jun 2017.

[9] Jiangang Li, Guangnan Luo, Rui Ding, Damao Yao, Junling Chen, Lei Cao, Jiansheng Hu, and Qiang Li and. Plasma facing components for the experimental advanced superconducting tokamak and CFETR. *Physica Scripta*, T159:014001, apr 2014.

[10] V. Philipps. Tungsten as material for plasma-facing components in fusion devices. *Journal of*

Nuclear Materials, 415(1):2–9, 2011.

[11] JW Coenen, S Antusch, M Aumann, W Biel, J Du, J Engels, S Heuer, A Houben, T Hoeschen, B Jasper, et al. Materials for DEMO and reactor applications—boundary conditions and new concepts. *Physica Scripta*, 2016(T167):014002, dec 2016.

[12] Y. Ueda, K. Schmid, M. Balden, W. Coenen J., T. Loewenhoff, A. Ito, A. Hasegawa, c. Hardie, M. Porton, and M. Gilbert. Baseline high heat flux and plasma facing materials for fusion. *Nuclear Fusion*, 57(9):092006, jun 2017.

[13] Christian Bachmann, G. Aiello, R. Albanese, R. Ambrosino, F. Arbeiter, J. Aubert, L. Boccaccini, D. Carloni, G. Federici, U. Fischer, M. Kovari, A. Li Puma, A. Loving, I. Maione, M. Mattei, G. Mazzone, B. Meszaros, I. Palermo, P. Pereslavtsev, V. Riccardo, P. Sardain, N. Taylor, S. Villari, Z. Vizvary, A. Vaccaro, E. Visca, and R. Wenninger. Initial {DEMO} tokamak design configuration studies. *Fusion Engineering and Design*, 98-99:1423–1426, October 2015.

[14] J.W. Coenen, Y. Mao, S. Sistla, A.v. Müller, G. Pintsuk, M. Wirtz, J. Riesch, T. Hoeschen, A. Terra, J.-H. You, H. Greuner, A. Kreter, Ch. Broeckmann, R. Neu, and Ch. Linsmeier. Materials development for new high heat-flux component mock-ups for DEMO. *Fusion Engineering and Design*, 146:1431–1436, feb 2019.

[15] H. Gietl, J. Riesch, J.W. Coenen, T. Höschen, and R. Neu. Production of tungsten-fibre reinforced tungsten composites by a novel continuous chemical vapour deposition process. *Fusion Engineering and Design*, 146:1426–1430, apr 2019.

[16] Y. Mao, J. W. Coenen, J. Riesch, S. Sistla, C. Chen, Y. Wu, L. Raumann, R. Neu, C. Linsmeier, and C. Broeckmann. *Spark Plasma Sintering Produced W-Fiber-Reinforced Tungsten Composites*, pages 239–261. Springer International Publishing, 2019.

[17] J Riesch, A Feichtmayer, M Fuhr, J Almanstötter, J W Coenen, H Gietl, T Höschen, Ch Linsmeier, and R Neu. Tensile behaviour of drawn tungsten wire used in tungsten fibre-reinforced tungsten composites. *Physica Scripta*, T170:014032, oct 2017.

[18] J. Mukerji. Ceramic matrix composites . *Defence Science Journal*, 43(4):385–395, jan 1993.

[19] PJ Chappell. Reinforcement-matrix interface effects in metal matrix composites. Technical report, MATERIALS RESEARCH LABS ASCOT VALE (AUSTRALIA), 1989.

[20] M.E.a Launey and R.O.a b Ritchie. On the fracture toughness of advanced materials. *Advanced Materials*, 21(20):2103–2110, 2009.

[21] Gergely Czel and M.R. Wisnom. Demonstration of pseudo-ductility in high performance

glass/epoxy composites by hybridisation with thin-ply carbon prepreg. *Composites Part A: Applied Science and Manufacturing*, 52(0):23–30, 2013.

[22] Kazuya Shimoda, Joon-Soo Park, Tatsuya Hinoki, and Akira Kohyama. Influence of pyrolytic carbon interface thickness on microstructure and mechanical properties of SiC/sic composites by {NITE} process. *Composites Science and Technology*, 68(1):98–105, 2008.

[23] A.S. Argon, editor. *Topics in Fracture and Fatigue*. Springer New York, 2012.

[24] Konstantinos G. Dassios. A review of the pull-out mechanism in the fracture of brittle-matrix fibre-reinforced composites. *Advanced Composites Letters*, 16(1):096369350701600, jan 2007.

[25] J Lamon. Interfaces and interfacial mechanics: influence on the mechanical behavior of ceramic matrix composites (cmc). *Le Journal de Physique IV*, 3(C7):C7–1607, 1993.

[26] JP Parmigiani and MD Thouless. The roles of toughness and cohesive strength on crack deflection at interfaces. *Journal of the Mechanics and Physics of Solids*, 54(2):266–287, 2006.

[27] H Gietl, A v Müller, JW Coenen, M Decius, D Ewert, T Höschen, Ph Huber, M Milwich, J Riesch, and R Neu. Textile preforms for tungsten fibre-reinforced composites. *Journal of Composite Materials*, 52(28):002199831877114, apr 2018.

[28] J. Riesch, J.-Y. Buffiere, T. Hoeschen, M. di Michiel, M. Scheel, Ch. Linsmeier, and J.-H. You. In situ synchrotron tomography estimation of toughening effect by semi-ductile fibre reinforcement in a tungsten-fibre-reinforced tungsten composite system. *Acta Materialia*, 61(19):7060–7071, 2013.

[29] J Riesch, T Hoeschen, Ch Linsmeier, S Wurster, and J-H You. Enhanced toughness and stable crack propagation in a novel tungsten fibre-reinforced tungsten composite produced by chemical vapour infiltration. *Physica Scripta*, 2014(T159):014031, 2014.

[30] L. Raumann, J.W. Coenen, J. Riesch, Y. Mao, H. Gietl, T. Höschen, Ch. Linsmeier, and O. Guillon. Modeling and validation of chemical vapor deposition of tungsten for tungsten fiber reinforced tungsten composites. *Surface and Coatings Technology*, jul 2019.

[31] B. Jasper, S. Schoenen, J. Du, T. Hoeschen, F. Koch, Ch. Linsmeier, R. Neu, J. Riesch, A. Terra, and J.W. Coenen. Behavior of tungsten fiber-reinforced tungsten based on single fiber push-out study. *Nuclear Materials and Energy*, 9:416–421, may 2016.

[32] B. Jasper et al. Powder metallurgical tungsten fiber-reinforced tungsten. *Material Science Forum, Trans Tech Publications*, 825-826:125–133, 2015.

[33] Y. Mao, J.W. Coenen, J. Riesch, S. Sistla, J. Almanstötter, B. Jasper, A. Terra, T. Höschen,

H. Gietl, Ch. Linsmeier, and C. Broeckmann. Influence of the interface strength on the mechanical properties of discontinuous tungsten fiber-reinforced tungsten composites produced by field assisted sintering technology. *Composites Part A: Applied Science and Manufacturing*, jan 2018.

[34] J. Riesch, M. Aumann, J.W. Coenen, H. Gietl, G. Holzner, T. Hoeschen, P. Huber, M. Li, Ch. Linsmeier, and R. Neu. Chemically deposited tungsten fibre-reinforced tungsten – the way to a mock-up for divertor applications. *Nuclear Materials and Energy*, 9:75–83, may 2016.

[35] J Riesch, Y Han, J Almanstötter, JW Coenen, T Höschen, B Jasper, P Zhao, Ch Linsmeier, and R Neu. Development of tungsten fibre-reinforced tungsten composites towards their use in DEMO—potassium doped tungsten wire. *Physica Scripta*, T167(T167):014006, jan 2016.

[36] H Gietl, J Riesch, JW Coenen, T Höschen, Ch Linsmeier, and R Neu. Tensile deformation behavior of tungsten fibre-reinforced tungsten composite specimens in as-fabricated state. *Fusion Engineering and Design*, 124:396–400, mar 2017.

[37] Y Mao, J W Coenen, J Riesch, S Sistla, J Almanstötter, B Jasper, A Terra, T Höschen, H Gietl, M Bram, J Gonzalez-Julian, Ch Linsmeier, and C Broeckmann. Development and characterization of powder metallurgically produced discontinuous tungsten fiber reinforced tungsten composites. *Physica Scripta*, T170:014005, aug 2017.

[38] J.W. Coenen, J. Riesch, J-H You, M. Rieth, G. Pintsuk, H. Gietl, B. Jasper, F. Klein, A. Litnovsky, Y. Mao, et al. Advanced materials for a damage resilient divertor concept for DEMO: Powder-metallurgical tungsten-fibre reinforced tungsten. *Fusion Engineering and Design*, 124:964–968, dec 2017.

[39] Y Mao, J Engels, A Houben, M Rasinski, J Steffens, A Terra, Ch Linsmeier, and JW Coenen. The influence of annealing on yttrium oxide thin film deposited by reactive magnetron sputtering: Process and microstructure. *Nuclear Materials and Energy*, 10:1–8, jan 2017.

[40] J.W. Coenen, Y. Mao, S. Sistla, J. Riesch, T. Hoeschen, Ch. Broeckmann, R. Neu, and Ch. Linsmeier. Improved pseudo-ductile behavior of powder metallurgical tungsten short fiber-reinforced tungsten (wf / w). *Nuclear Materials and Energy*, 15:214–219, may 2018.

[41] A. v. Müller, M. Ilg, H. Gietl, T. Höschen, R. Neu, G. Pintsuk, J. Riesch, U. Siefken, and J.H. You. The effects of heat treatment at temperatures of 1100c to 1300c on the tensile properties of high-strength drawn tungsten fibres. *Nuclear Materials and Energy*, 16:163–167, aug 2018.

[42] H Bolt, V Barabash, G Federici, J Linke, A Loarte, J Roth, and K Sato. Plasma facing and

high heat flux materials - needs for ITER and beyond. *Journal of Nuclear Materials*, 307, Part 1(0):43–52, 2002.

[43] Xunxiang Hu, Takaaki Koyanagi, Makoto Fukuda, NAP Kiran Kumar, Lance L Snead, Brian D Wirth, and Yutai Katoh. Irradiation hardening of pure tungsten exposed to neutron irradiation. *Journal of Nuclear Materials*, 480:235–243, nov 2016.